3-Fluoro-2,4-dioxa-3-phosphadecalins as Inhibitors of Acetylcholinesterase. A Reappraisal of Kinetic Mechanisms and Diagnostic Methods

by **Antonio Baici***[a]), **Patricia Schenker**[a]), **Michael Wächter**[b]), and **Peter Rüedi***[b])

[a]) Biochemisches Institut der Universität Zürich, Winterthurerstrasse 190, CH-8057 Zürich
[b]) Organisch-chemisches Institut der Universität Zürich, Winterthurerstrasse 190, CH-8057 Zürich

A systematic survey of the acetylcholine-mimetic 2,4-dioxa-3-phosphadecalins as irreversible inhibitors of acetylcholinesterase revealed hitherto overlooked properties as far as the kinetic mechanisms of interaction are concerned. As a support to past and future work in this field, we describe the kinetics of eight reaction schemes that may be found in irreversible enzyme modification and compare them with two mechanism of reversible, slow-binding inhibition. The relevant kinetic equations and their associated graphical representations are given for all mechanisms, and concrete examples illustrate their practical use. Since irreversible inhibition is a time-dependent phenomenon, kinetic analysis is greatly facilitated by fitting the appropriate integrated rate equations to reaction-progress curves by nonlinear regression. This primary scrutiny provides kinetic parameters that are indispensable tools for diagnosing the kinetic mechanism and for calculating inhibition constants. Numerical integration of sets of differential equations is an additional useful investigation tool in critical situations, *e.g.*, when inhibitors are unstable and/or act as irreversible modifiers only temporarily.

1. Introduction. – In an earlier article [1], we have reported on the synthesis and characterization of the racemic *P(3)*-axially and *P(3)*-equatorially substituted *cis*- and *trans*-configured 2,4-dioxa-9-aza-, 2,4-dioxa-8-aza-, and 2,4-dioxa-7-aza-3-phosphabicyclo[4.4.0]decane 3-oxides (**I**–**III**, resp.; *Fig. 1*).

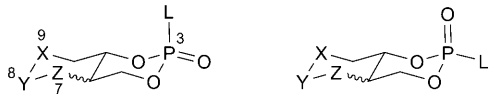

I X = NR, $\overset{\oplus}{N}R_2$, Y = Z = CH_2
II X = CH_2, Y = NR, $\overset{\oplus}{N}R_2$, Z = CH_2
III X = Y = CH_2, Z = NR, $\overset{\oplus}{N}R_2$
IV X = Y = Z = CH_2

L = electron-withdrawing group (F, Cl, Br, N_3, OR, NR_2, SR)

Fig. 1. *The 2,4-dioxa-3-phosphadecalins of types* **I**–**IV**

Being configuratively fixed and conformationally constrained P-analogues of acetylcholine (7-aza and 9-aza isomers) or γ-homoacetylcholine (8-aza isomers) (*Scheme 1*), these heterocycles represent acetylcholine mimetics, and they are

considered to be suitable for the investigation of molecular interactions with acetylcholinesterase (AChE), such as the recognition conformation of acetylcholine (ACh) and the stereochemistry of modification reactions[1]) of serine hydrolases. The related 3-fluoro- and 3-(2,4-dinitrophenoxy)-2,4-dioxa-3-phosphadecalins (type **IV**; *Fig. 1* and *Scheme 1*) have been successfully used as probes for the determination of the stereochemical course of the inhibition of δ-chymotrypsin [2] and the proof for the covalently phosphorylated enzyme [3] by ^{31}P-NMR spectroscopy. Enzyme-kinetic studies on the basis of a simplified approach according to *Scheme 2*[2]) had revealed that many of the prepared organophosphates of type **I**–**IV** (*Fig. 1*) are inhibitors of AChE [8–12] (*Scheme 2*), and preliminary results have been summarized [13]. However, during the past years, we have encountered significant inconsistencies concerning the reproducibility of the kinetic data of the phosphadecalins. Meanwhile, we have synthesized all the optically active (ee > 99%) organophosphates of type **I**–**IV** (L = F; *Scheme 1*), and the mentioned problems prompted us to start a thorough reinvestigation to find and apply an appropriate enzyme-kinetic system that is generally applicable to our compounds, providing reliable results.

2. Reappraisal of Kinetic Mechanisms and Diagnostic Methods. – 2.1. *General.* Although apparently a simple theme, the reaction of an enzyme with a substrate and/or an inhibitor to yield products or a modified enzyme species, is a highly complex cycle with multiple equilibria and accordingly complex rate parameters. As a matter of fact, there exists no analytical solution for the exact description of the general case [15][16]. Despite this inherent complexity, the kinetics of irreversible enzyme modification has been the subject of early studies, in which discontinuous methods were used for measuring residual enzyme activity after preincubating the enzyme of interest with modifiers [17–19]. More recently, continuous methods gained popularity because of the large information contained in progress curves obtained by monitoring the appearance of product following the hydrolysis of a chromogenic or fluorogenic substrate [20–23]. However, modifier instability and temporary inhibition constitute serious drawbacks for the practical use of many compounds, and represent a dilemma

---

[1]) The term 'modification' comprises all types of chemical interactions with enzymes and is not limited to inhibition reactions. Hence, it is more appropriate in the present re-evaluation that constitutes a general approach.

[2]) In most enzyme-kinetic studies on organophosphorus inhibitors of esterases, only the overall process is considered (*Scheme 2*). We relied on the basic procedure introduced by *Aldridge* [4] and later refined by *Main* and *Dauterman* [5], and *Hart* and *O'Brien* [6]. As our primary goal was the search for strong inhibitors with respect to their applicability for ^{31}P-NMR studies [2][3], we used these simplified, straightforward protocols that were applied at that time by several research groups (*e.g.*, [7]). For detailed experimental descriptions, representative calculations, and results, see [2][8–13]. Racemic 3-phosphadecalins with the following leaving groups have been prepared and tested (see *Scheme 1*): L = F [1][8][11–13] (types **I**–**IV**), Cl [1][8–10] (types **I**, **II**, and **IV**), Br, N_3 [8] (type **IV**), 4-nitrophenoxy [1][9][10] (types **I** and **II**), 2,4-dinitrophenoxy [1][8–10] (types **I**, **II**, and **IV**), OR [8][9] (types **I**, **II**, and **IV**), NR_2 [8] (type **IV**), and SR [8] (type **IV**). Remarkably, the *N,N*-dimethylammonium compounds ($R^1 = R^2 = Me$, L = Cl, 4-nitrophenoxy, 2,4-dinitrophenoxy) that constitute the most close mimetics were weak reversible inhibitors [10] (types **I** and **II**). For a compilation of the applied procedures, experimental conditions, cross-comparisons, and a critical discussion of the respective results, see [14].

Scheme 1. *The Basic Concept of the Organophosphorus Acetylcholine Mimetics*

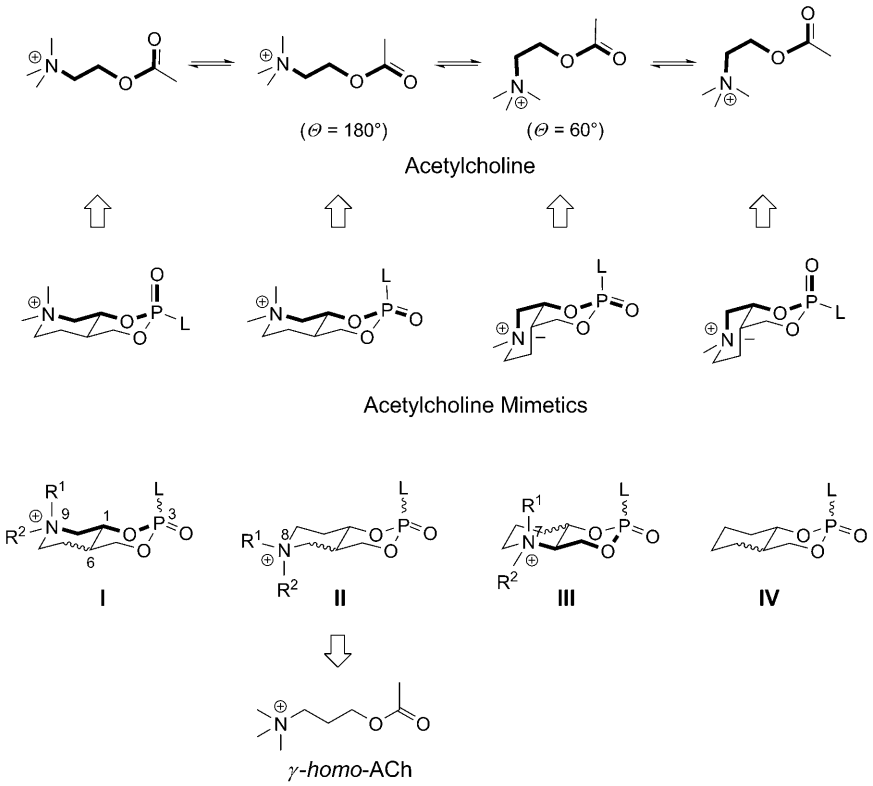

Each structural type, **I** – **IV**: *cis*-, *trans*-, axially, and equatorially P-substituted isomers
R = (*tert*-amines, free bases), H, Me, CH_2Ph; $R^1 = R^2$ or $R^1 \neq R^2$

Scheme 2. *The Simplified Kinetic Approach*

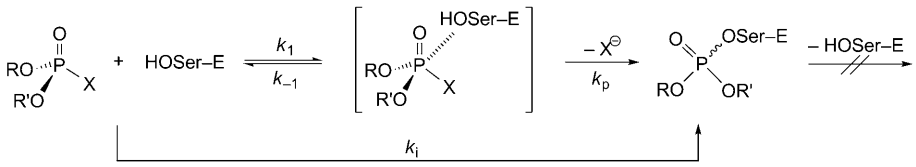

E = Enzyme: Serine hydrolase (acetylcholinesterase, chymotrypsin)
k_1,k_{-1}: Rate constants (also referred to as k_{on} and k_{off}, resp.)
$k_{-1}/k_1 = K_D$: Dissociation constant
k_p: Phosphorylation constant (also referred to as association constant, k_{ass})
$k_i = k_p/K_D$: Overall inhibitory potency ('bimolecular reaction constant')

for the kinetic interpretation of experimental data. In fact, when a continuous progress curve method for data acquisition is used, temporary inhibition and modifier instability can be mistaken for true reversibility of the reaction. In this article, we reconsider and discuss diagnostic criteria for distinguishing mechanisms of enzyme inhibition based on the analysis of progress curves. We will consider only inhibitors of the competitive type, *i.e.*, those that bind to free enzyme, not to the enzyme–substrate complex.

2.2. *Theoretical Considerations.* 2.2.1. *Reversible, Slow-Binding Inhibition*. For the purposes of the discussion that will follow on irreversible enzyme modification, it is useful to examine first the behavior of reversible, slow-acting inhibitors. *Scheme 3* shows two common mechanisms, **2A-R** and **1A-R**, of reversible, slow-binding inhibition. In mechanism **2A-R**, slow production of an enzyme–inhibitor complex ($E \cdot I$)[3]) is preceded by a rapid equilibration between E and I to form an adsorptive complex (EI). Mechanism **1A-R** is a degenerated form of mechanism **2A-R**, in which the concentration of EI is kinetically insignificant. Slow-binding, slow, tight-binding inhibition, and irreversible enzyme modification are time-dependent phenomena, *i.e.*, the final species do not form instantaneously, but in the range of minutes to hours. Apart from its physiological and pharmacological significance, this behavior offers a handy tool for measuring the kinetic parameters and for determining the respective inhibition mechanism. For such slow processes, the integrated rate equation, expressed as product concentration *vs.* time, takes the general form (*Eqn. 1* in *Table 1*). The term v_s represents the rate after attainment of the steady-state, and v_z (for zero time) corresponds to the rate at $t=0$. We purposely use the symbol v_z in the case of slow enzyme-modification reactions as a distinction from v_0, which is used to represent the rate in the absence of modifiers. Depending on the experimental conditions and mechanism, v_z can be greater or less than v_s, and it can be equal to or less than v_0. The first-order rate constant λ that describes the approach to the steady-state has a characteristic expression for each mechanism. The parameter d (displacement) is introduced in *Eqn. 1* (*Table 1*), and other forms of this equation to take into account product present before the start of the reaction or any spectroscopic signal proportional

Scheme 3. *Reversible, Slow-Binding Enzyme Inhibition.* These are the reversible counterparts (**R** indicates reversibility) of mechanisms **2A** (*Scheme 4*) and **1A** (*Scheme 5*), respectively.

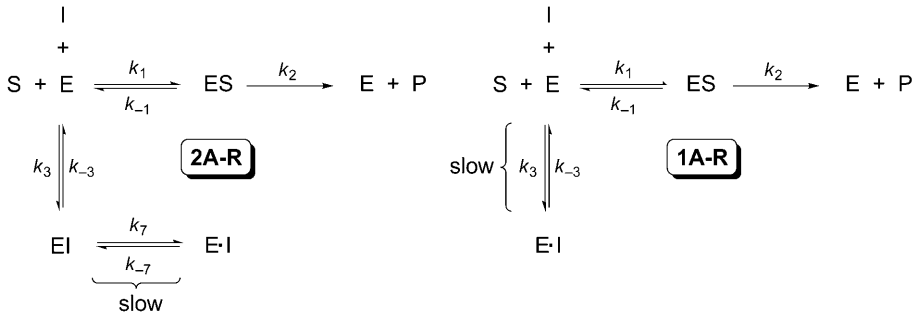

[3]) For a list of the symbols, see the *Appendix*.

Table 1. *Equations for Mechanisms* **2A-R** *and* **1A-R** (*cf. Scheme 3*). The expressions v_z and v_s apply to assays in which the reaction is started by adding the enzyme to a solution containing substrate and inhibitor.

Mechanism **2A-R**		Mechanism **1A-R**	
$[P] = v_s t + \frac{(v_z - v_s)(1 - e^{-\lambda t})}{\lambda} + d$	(1)	[P] as *Eqn. 1*	
$\lambda = k_{-7} + \frac{k_7[I]}{K_i\left(1 + \frac{[S]}{K_m}\right) + [I]}$ $K_i = \frac{k_{-3}}{k_3}$	(2)	$\lambda = k_{-3} + \frac{k_3[I]}{1 + \frac{[S]}{K_m}}$	(3)
$v_z = \frac{V[S]}{K_m\left(1 + \frac{[I]}{K_i}\right) + [S]}$	(4)	$v_z = v_0 = \frac{V[S]}{K_m + [S]}$	(5)
$v_s = \frac{V[S]}{K_m\left(1 + \frac{[I]}{K_i\left(\frac{k_{-7}}{k_7 + k_{-7}}\right)}\right) + [S]}$	(6)	$v_s = \frac{V[S]}{K_m\left(1 + \frac{[I]}{K_i}\right) + [S]}$	(7)

to it, which may be non-zero at the beginning of the reaction. *Eqn. 1* was originally derived for describing the concept of enzyme hysteresis [24], and was later used for characterizing slow-binding inhibition [25][26]. It applies to reactions in which enzymes respond slowly to a rapid change in the concentration of any modifier.

2.2.2. *Enzyme Inactivation; Irreversible Inhibition*[4]). In most cases, the kinetics of irreversible enzyme inhibition can be described by mechanism **2A** (*Scheme 4*). Mechanism **2A** consists in the formation of a fast-equilibrating adsorptive complex (EI), followed by a slow step in which the enzyme is irreversibly converted to a covalently modified enzyme (E–I), and thereby inactivated. The concentration of the reversible adsorptive intermediate may be kinetically insignificant, meaning that the dissociation constant $K_i = k_{-3}/k_3$ may be high with respect to the concentration of inhibitor used in the experiments; in this case, mechanism **2A** degenerates to mechanism **1A** (*Scheme 5*). While there is no reason for considering these two mechanisms as being chemically different (as is also for mechanisms **2A-R** and **1A-R**; *Scheme 3*), a distinction is made merely for practical purposes and mathematical convenience.

---

4) The term '*inactivation*' specifically indicates that a modifier covalently converts the enzyme to a species devoid of catalytic activity. The expression is preferentially used by the specialists in place of '*irreversible inhibition*' to distinguish reversibility and irreversibility at a glance. Although less accurate, the classical term '*irreversible inhibitor*', is retained in this article due to practical reasons.

Scheme 4. *Mechanisms for Two-Step Irreversible Enzyme Modification.* In the four variants of this mechanism (the number **2** denotes a two-step inhibition process), covalent enzyme modification (E–I) is preceded by the reversible formation of an adsorptive complex EI. Mechanism **2B** describes an unstable modifier, which undergoes spontaneous, nonenzymatic decomposition. Mechanism **2C** shows temporary inhibition, in which the inhibited enzyme decays to free enzyme, which is recycled, and an inert species I*. Mechanism **2D** illustrates the case of a chemically unstable modifier, which, at the same time, exerts temporary inhibition. I′ and I* do no longer affect enzyme activity and are withdrawn from the system.

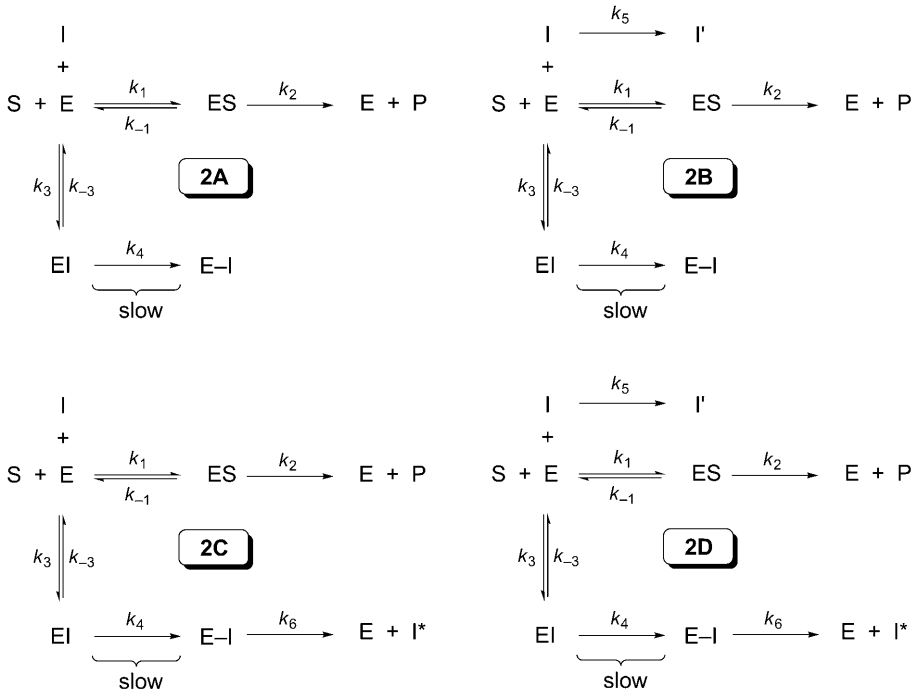

Often, molecules designed as irreversible modifiers of enzyme activity undergo spontaneous, nonenzymatic decomposition, usually by hydrolysis to an inert species (I′; mechanisms **2B** (*Scheme 4*) and **1B** (*Scheme 5*)). Other molecules act as temporary inhibitors, meaning that free enzyme and an enzymatically cleaved form of the modifier (I*) are generated (mechanisms **2C** (*Scheme 4*) and **1C** (*Scheme 5*)). In the worst case, a compound can be unstable and temporary as well (mechanisms **2D** (*Scheme 4*) and **1D** (*Scheme 5*)). In the same way as reversible inhibitors, enzyme inhibitors can be competitive, uncompetitive, or mixed-type. The latter is a blend of competitive and uncompetitive character [20]. In the case of genuinely irreversible processes, the steady-state rate v_s in *Eqn. 1* (*Table 1*) is set to zero, and the rate is expressed by *Eqn. 8* (*Table 2*).

For reasons of convenience, expressions which are found in the literature (*e.g.*, [16]) are summarized for reversible mechanisms (*Table 1*), for irreversible mechanisms in two steps (*Table 2*), and for irreversible mechanisms in one step (*Table 3*). To the best of our knowledge, analytical expressions have not been published for the temporary

Scheme 5. *Mechanisms for One-Step Irreversible Enzyme Modification.* In these mechanisms (the number **1** denotes one-step inhibition), enzyme and modifier form covalently inhibited E–I in a bimolecular reaction. The unstable inhibitor (**1B**), temporary inhibition (**1C**), and a blend of these two variants of the mechanism (**1D**) are analogous to the corresponding panels in *Scheme 4.*

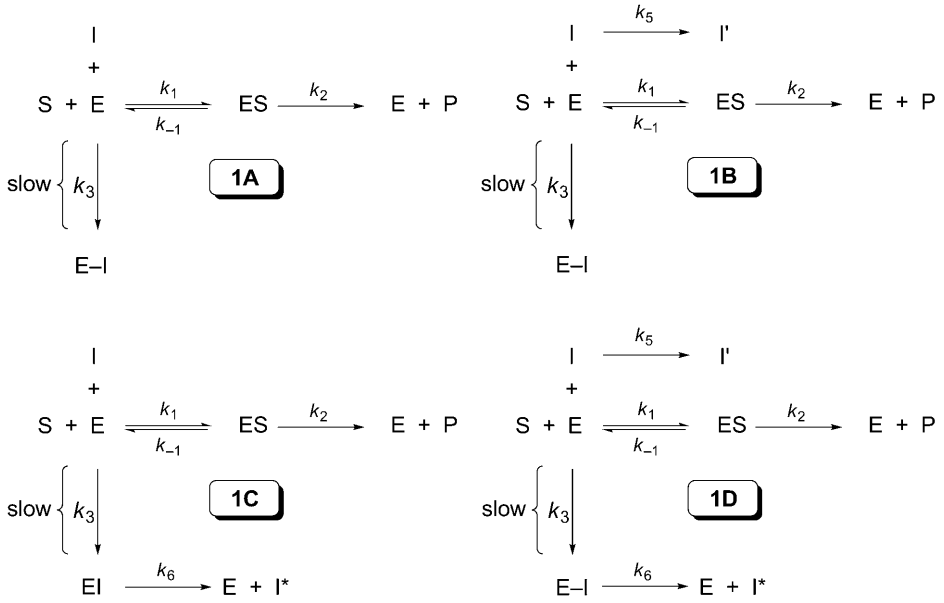

Table 2. *Equations for Mechanisms* **2A** *and* **2C** (*cf. Scheme 4*). The expressions v_z and v_∞ apply to assays in which the reaction is started by adding the enzyme to a solution containing substrate and inhibitor.

Mechanism **2A**		Mechanism **2C**	
$[P] = \frac{v_z}{\lambda}(1 - e^{-\lambda t}) + d$	(8)	$[P] = v_\infty t + \frac{v_z - v_\infty}{\lambda}(1 - e^{-\lambda t}) + d$	(9)
$\lambda = \frac{k_4[I]}{K_i\left(1 + \frac{[S]}{K_m}\right) + [I]}$	(10)	$\lambda = k_6 + \frac{k_4[I]}{K_i\left(1 + \frac{[S]}{K_m}\right) + [I]}$	(11)
$K_i = \frac{k_{-3}}{k_3}; \quad k_i = \frac{k_4}{K_i}$		$K_i = \frac{k_{-3}}{k_3}; \quad k_i = \frac{k_4}{K_i}$	
$v_z = \frac{V[S]}{K_m\left(1 + \frac{[I]}{K_i}\right) + [S]}$	(4)	v_z as for mechanism **2A**	
$v_\infty = 0$		$v_\infty = \frac{V[S]}{K_m\left(1 + \frac{[I]}{K_i}\left(1 + \frac{k_4}{k_6}\right)\right) + [S]}$	(12)

mechanisms **2C** (*Scheme 4* and *Table 2*) and **1C** (*Scheme 5* and *Table 3*) with explicit expressions in the style used in this article. The symbol v_∞ in these *Tables* is the counterpart of v_s in *Table 1*. The infinity subscript solely indicates that this rate is calculated at the end of the exponential phase, a condition mathematically obtained by setting $t = \infty$ in the expression $e^{-\lambda t}$.

Table 3. *Equations for Mechanisms* **1A** *and* **1C** (*cf. Scheme 5*). The expressions of v_z and v_∞ apply to assays in which the reaction is started by adding the enzyme to a solution containing substrate and inhibitor.

Mechanism **1A**		Mechanism **1C**	
$[P] = \frac{v_z}{\lambda}(1 - e^{-\lambda t}) + d$	(8)	$[P] = v_\infty t + \frac{v_z - v_\infty}{\lambda}(1 - e^{-\lambda t}) + d$	(9)
$\lambda = \frac{k_3[I]}{1 + \frac{[S]}{K_m}}$	(13)	$\lambda = k_6 + \frac{k_3[I]}{1 + \frac{[S]}{K_m}}$	(14)
$v_z = v_0 = \frac{V[S]}{K_m + [S]}$	(5)	v_z as for mechanism **1A**	
$v_\infty = 0$		$v_\infty = \frac{V[S]}{K_m\left(1 + \frac{k_3}{k_6}[I]\right) + [S]}$	(15)

A complete treatment of mechanisms **2B** (*Scheme 4*) and **1B** (*Scheme 5*) for unstable inhibitors was published by *Topham* in a comprehensive theoretical treatment that also included partial inhibitors as well as activators [23]. This valuable article, in which an impeccable mathematical language was used, may possibly be difficult for end users less familiar with this topic. Therefore, this treatment is summarized below for mechanism **1B** to show conceptual differences with integrated rate equations for systems **2A**, **2C**, **1A**, and **1C**, and to explain how to deal in practice with unstable modifiers. The complex integrated rate equation for mechanism **2B** will not be treated here because its solution is only possible under special circumstances [23]. In the case of either mechanism **2D** or **1D**, it is questionable whether the compounds under investigation should still be called inhibitors. Although integrated rate equations for these mechanisms can be derived, their concrete application to real cases is mathematically laborious, and the results are mere of academic interest.

2.2.3. *Discrimination of Mechanisms.* To provide a convenient reference for diagnostic purposes, progress curves for the mechanisms shown in this article were simulated by numerical integration of the appropriate sets of differential equations. All calculated and experimental curves shown below refer to reactions started by adding enzyme to a solution containing substrate and inhibitor. The differential diagnosis of the mechanisms is accomplished by inspection of the shapes of the progress curves, and by analysis of the dependencies of λ and velocities on inhibitor concentration.

Progress curves for mechanisms **2A-R** and **1A-R**, as well as the dependencies of the parameters λ, v_z, and v_s on [I], are shown in *Fig. 2*. Distinguishing mechanism **2A-R**

from its counterpart **1A-R** is straightforward, since the dependency of λ on [I] is hyperbolic for mechanism **2A-R** and linear for mechanism **1A-R**. Furthermore, v_z decreases hyperbolically with [I], or is independent of [I] for mechanisms **2A-R** and **1A-R**, respectively. Individual kinetic constants can be calculated from the plots of λ *vs.* [I], as shown in *Fig. 2*. From the fits of v_z and v_s, K_i, as well as the overall inhibition constant $(K_i k_{-7})/(k_7+k_{-7})$, for mechanism **2A-R** can be calculated and used to check the internal consistency with results from the λ *vs.* [I] plot.

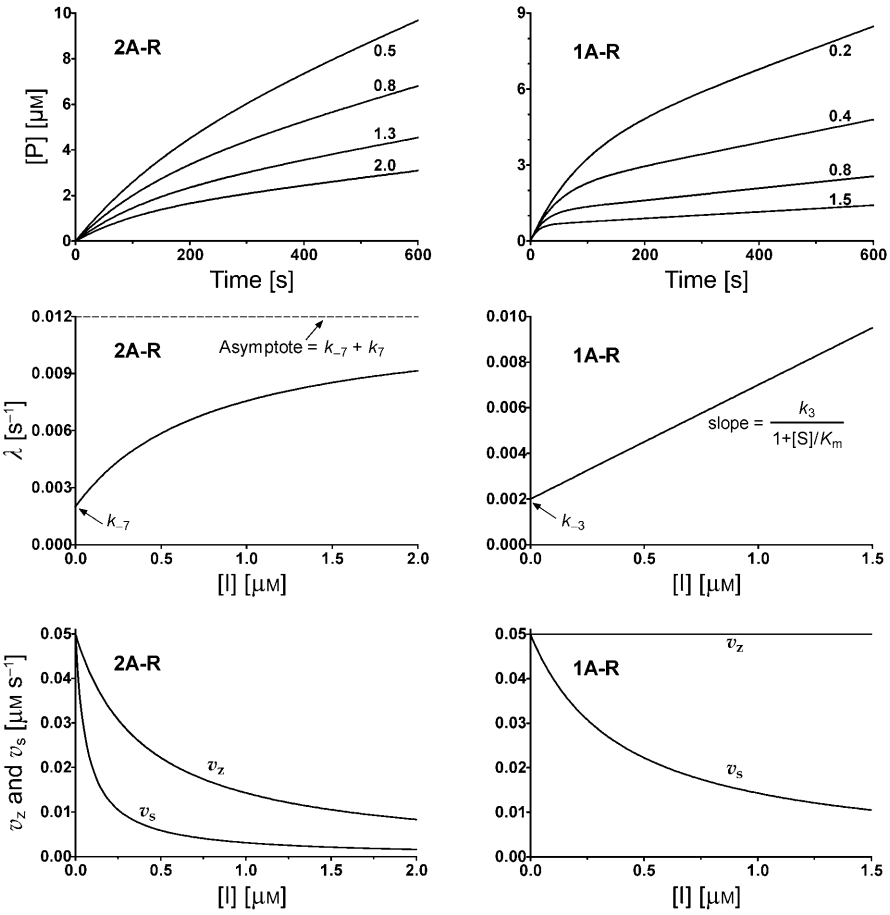

Fig. 2. *Progress curves and diagnostic parameters for mechanisms* **2A-R** *and* **1A-R** (*cf. Scheme 3*). Numbers next to the curves in the top panels indicate inhibitor concentrations (μM). Curves were generated with the following parameters common to both mechanisms: $k_2=20\ s^{-1}$, $[E]_t=5$ nM, $[S]=K_m=100$ μM; for mechanism **2A-R**: $k_3=0.5\ \mu M^{-1}\ s^{-1}$, $k_{-3}=0.2\ s^{-1}$, $k_7=0.01\ s^{-1}$, $k_{-7}=0.002\ s^{-1}$; for mechanism **1A-R**: $k_3=0.1\ \mu M^{-1}\ s^{-1}$, $k_{-3}=0.002\ s^{-1}$.

Mechanism **2A** for irreversible inhibition can unmistakably be distinguished from its reversible counterpart **2A-R**, if the progress curves can be measured for a sufficiently long time to allow complete inhibition. The irreversible mechanism is

characterized by an end value of progress curves parallel to the time axis, indicating that there is no steady-state with a positive slope (*Fig. 3*). Also, the ordinate intercept of λ *vs.* [I] is zero in this case, while it is non-zero for mechanism **2A-R**. A distinction of mechanism **2C** from **2A-R** is impossible, when only progress curves and the dependencies of parameters on [I] are considered. In fact, the positive slope described by v_∞ can be mistaken for the steady-state of a reversible system. Instead, this slope is determined by free enzyme that is recycled in the reaction following the breakdown of E–I. However, a reliable discrimination is possible by preincubating enzyme and inhibitor, and starting the reaction by adding substrate: for a reversible mechanism, the steady-state slope will be independent of the preincubation time, while, for mechanism **2C**, the slope will increase by increasing the preincubation time. This corresponds to the decreasing inhibitor concentration available to the enzyme.

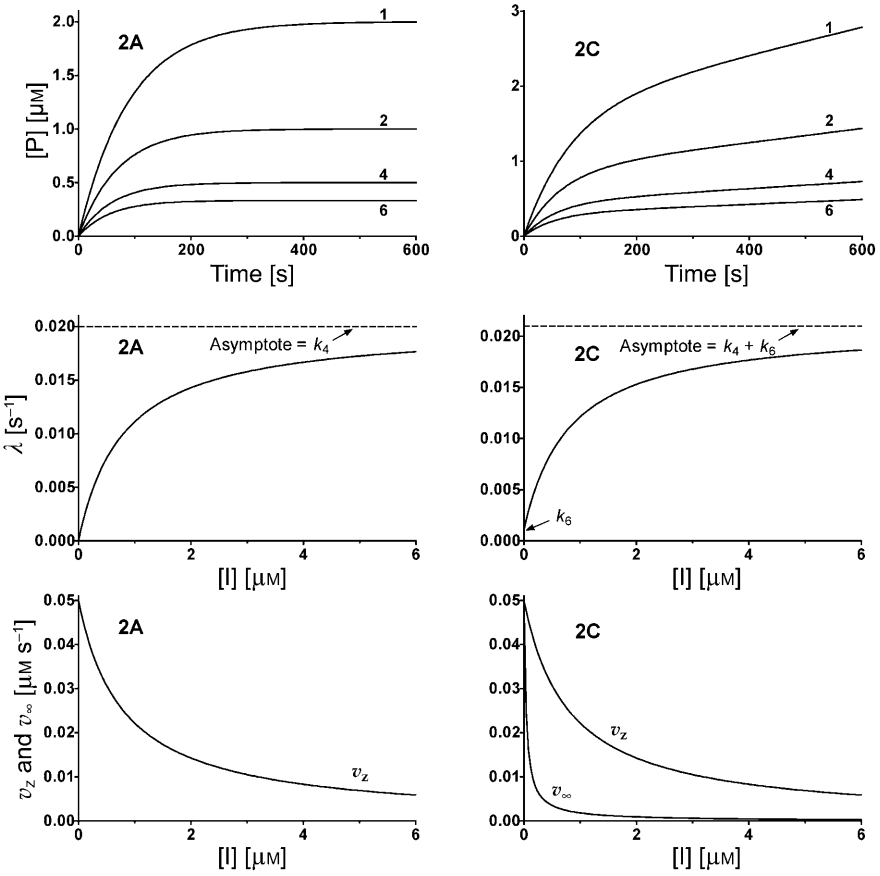

Fig. 3. *Progress curves and diagnostic parameters for mechanisms* **2A** *and* **2C** (*Scheme 4*). Numbers next to the curves in the top panels indicate inhibitor concentrations (μM). Curves were generated with the following parameters common to both mechanisms: $k_2 = 20\ s^{-1}$, $[E]_t = 5$ nM, $[S] = K_m = 100$ μM, $k_3 = 0.5\ \mu M^{-1}\ s^{-1}$, $k_{-3} = 0.2\ s^{-1}$, $k_4 = 0.02\ s^{-1}$; for mechanism **2C**: $k_6 = 0.001\ s^{-1}$.

Progress curves and parameter dependencies for mechanisms **1A** and **1C** are shown in *Fig. 4*. Diagnostic features of system **1A** are the reaction profiles ending up with slope zero and the linear dependency of λ on [I] with zero intercept on the ordinate. The non-zero intersection on the ordinate for mechanism **1C**, which corresponds to k_6, may not be accessible to unambiguous measurement, and its successful determination depends on data quality. A statistical test to evaluate a significant non-zero intercept will be very useful in this case. Also for mechanism **1C**, a definite distinction from mechanism **1A-R** is not possible from inspection of the graphics, but the preincubation method discussed above is reliable again.

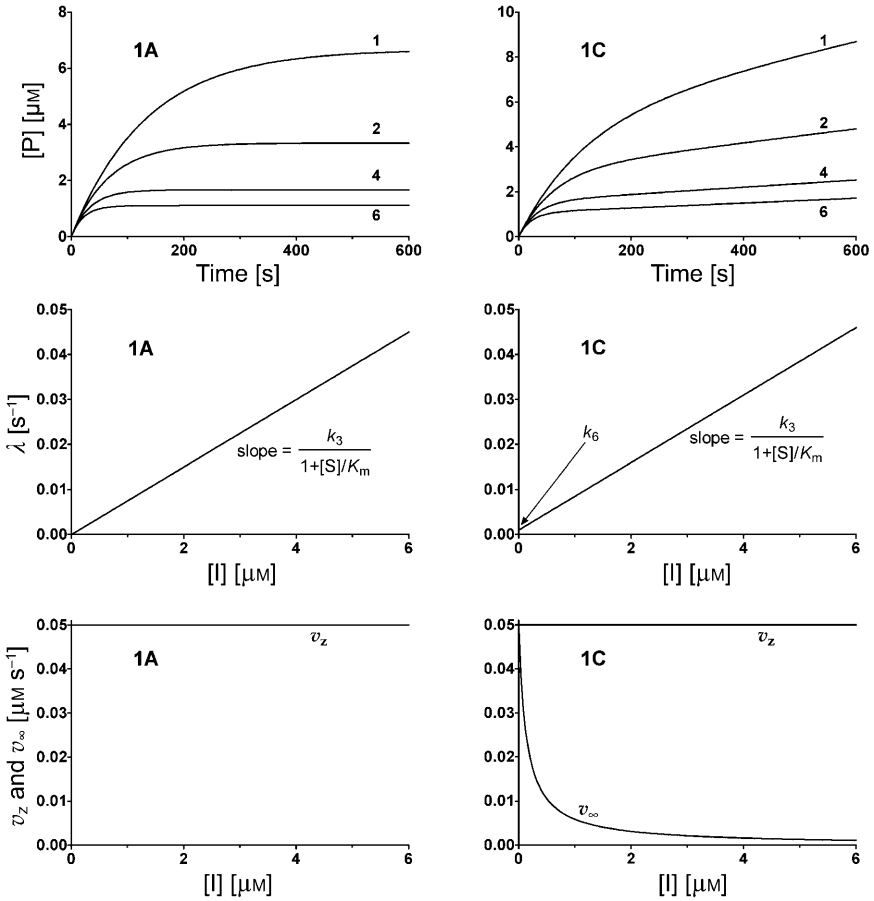

Fig. 4. *Progress curves and diagnostic parameters for mechanisms* **1A** *and* **1C** (*Scheme 5*). Numbers next to the curves in the top panels indicate inhibitor concentrations (μM). Curves were generated with the following parameters common to both mechanisms: $k_2 = 20\ s^{-1}$, $[E]_t = 5$ nM, $[S] = K_m = 100$ μM, $k_3 = 0.015\ \mu M^{-1}\ s^{-1}$; for mechanism **1C**: $k_6 = 0.001\ s^{-1}$.

2.2.4. *Inhibition by an Unstable Compound, Mechanism* **1B**. An analytical expression of λ does not exist for this model, because the concentration of the

inhibitor varies with time. However, an analytical expression for the integrated rate equation can be obtained upon *Maclaurin* series expansion [23]:

$$[\mathrm{P}] = \frac{v_z}{k_5} e^{-\left\{\frac{k_3 K_m [\mathrm{I}]_t}{k_5 (K_m + [\mathrm{S}])}\right\}} \left\{ k_5 t + \sum_{i=1}^{\infty} \left\{ \frac{k_3 K_m [\mathrm{I}]_t}{k_5 (K_m + [\mathrm{S}])} \right\}^i \frac{\left[1 - (e^{-k_5 t})^i\right]}{i \cdot i!} \right\} \qquad (16)$$

In *Eqn. 16*, $v_z = v_0$ (the rate in the absence of modifier), K_m can be evaluated from measurements performed with substrate alone, and $[\mathrm{I}]_t$ is the total inhibitor concentration introduced initially. Therefore, the rate constants k_3 and k_5 can be obtained by fitting this equation to progress curves by nonlinear regression. How many terms, denoted by the index *i* in *Eqn. 16*, should be used in the regression analysis depends on the value of k_5: a small value will require more terms than a large one. For instance, with $k_5 = 0.005\ \mathrm{s}^{-1}$, the third term is sufficient to fit a progress curve, while with $k_5 = 0.001\ \mathrm{s}^{-1}$, *Maclaurin* expansion till the 10th term is necessary. In turn, the last option can be used routinely.

Simulated progress curves for an unstable inhibitor obeying mechanism **1B** are shown in *Fig. 5* (*left panel*). These do not consist of a single exponential followed by a straight line parallel to the time axis as shown in the curve labeled $k_5 = 0$, which corresponds to a stable inhibitor. Instead, an increase of k_5 means an increase of the rate of degradation of the inhibitor to the inert species I′, as shown in *Fig. 5* (*right panel*). Thus, progress curves are similar to those obtained in the presence of a reversible inhibitor, and, for high values of k_5, I is degraded rapidly causing the progress curve to be linear. The straight line following the exponential phases in *Fig. 5* (*e.g.*, in the curve with $k_5 = 0.01\ \mathrm{s}^{-1}$) does not correspond to a steady-state but reflects the continuous decrease in the concentration of available inhibitor according to *Eqn. 16*. Attempting to fit either *Eqns. 8* or *9* to data obtained with unstable compounds results in inconsistent fittings with statistically meaningless results. This is due to the fact that

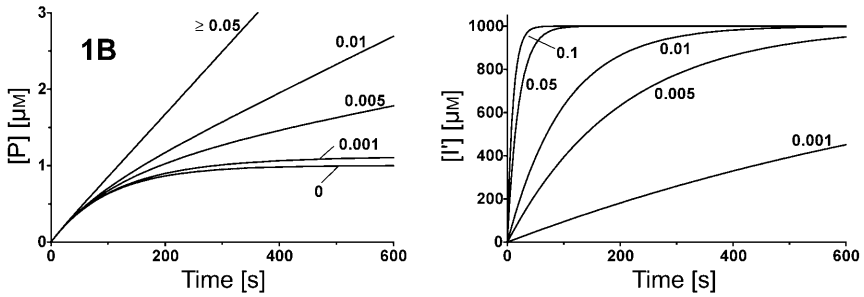

Fig. 5. *Progress curves for an unstable inhibitor, mechanism* **1B** (*Scheme 5*). *Left:* Progress curves. *Right:* concentration of the chemically inert inhibitor, I′. Curves were simulated by numerical integration with *Matlab–Simulink* software (www.mathworks.com) using the following parameters: $k_2 = 0.2\ \mathrm{s}^{-1}$, $k_3 = 10\ \mathrm{M}^{-1}\ \mathrm{s}^{-1}$, $K_m = 1$ mM, $[\mathrm{S}] = 1$ mM, $[\mathrm{E}]_t = 100$ nM, $[\mathrm{I}]_t = 1$ mM, k_5 from 0 to $0.1\ \mathrm{s}^{-1}$ as shown (numbers next to the curves). For $k_5 = 0$, there is no production of I′, and the progress curve corresponds to that of mechanism **1A** (*Fig. 4* and *Scheme 5*).

the condition of constant [I] during the measurement time, necessary for integrating the rate equation, is violated. This represents a valuable diagnostic tool for differentiating **1B** from other mechanisms. Progress curves for an unstable inhibitor obeying mechanism **1B** are very similar to those of mechanisms **1A-R** and **1C**. Discrimination is possible by preincubating the inhibitor in assay buffer for 2–3 periods of time. Then, substrate is added followed by enzyme: for both mechanisms **1A-R** and **1C**, the reaction profiles will be independent on preincubation time, but rate will increase with the preincubation time in the case of mechanism **1B**, reflecting disappearance of inhibitor through hydrolysis. If all inhibitor undergoes hydrolysis during preincubation the rate returns to control values (slope of the curve as shown for $k_5 \geq 0.05\ s^{-1}$ in *Fig. 5* (*left panel*). For very low values of k_5, the instability of the inhibitor may not be appreciable in a dynamic assay over a relatively short time (*e.g.*, curve for $k_5 = 0.001\ s^{-1}$).

To summarize, the concept highlights the importance of progress curves as a means for discriminating among mechanisms and for calculating the second-order inhibition constants. The progress-curve method offers many practical and statistical advantages over previous methods [4–7]. After choosing an appropriate substrate that allows continuous detection of reaction progress, and knowing the kinetic parameters V and K_m for this substrate, data collection consists in continuously recording the appearance of product at a fixed substrate and enzyme concentration for several concentrations of the inhibitor. The competitive or other character of the inhibitor can be ascertained by collecting data at various substrate concentrations. *Eqns. 8* or *9* are fitted to each experimental curve by nonlinear regression to calculate λ, v_z, and v_∞ as appropriate, which are then plotted against the inhibitor concentration for establishing the mechanism and calculating the relevant kinetic parameters. A hyperbola or a straight line passing through the origin of the axes is diagnostic for mechanisms **2A** and **1A**, respectively. As a caveat, irreversible enzyme inhibition and reversible slow, tight-binding inhibition can hardly be distinguished from one another by this method. However, in slow, tight-binding inhibition saturation will occur at total inhibitor concentrations of the same order of magnitude as the total enzyme concentration $[E]_t$ used in the assays, while in irreversible inhibition this will usually occur at $[I]_t \gg [E]_t$.

3. Representative Examples. – The application of the concept presented above furnished reproducible and consistent kinetic data of our 2,4-dioxa-3-phosphadecalins of the types **I**–**IV** (*Fig. 1* and *Scheme 1*). In the following, selected representative results that clearly illustrate the convenient practice of the protocol are presented (structures in *Fig. 6*, and kinetic constants in *Table 4*). The inhibition experiments of AchE with the organophosphorus compounds were performed by means of the *Ellman* assay [27] at pH 7.00 ± 0.02 in the presence of substrate (acetylthiocholine) and the chromogenic '5,5′-dithiobis(2-nitrobenzoic acid-3,3′-6)'. The progress curves were monitored at 410–414 nm (yellow dianion of 5-thio-2-nitrobenzoic acid, $\lambda_{max} = 412$ nm).

The comparison between **DFP** and a fully irreversible inhibitor, (−)-*trans*-**IVax**, is shown in *Fig. 7*. There are no diagnostic problems for these two inhibitors, for which the linear dependence of λ upon [I], with the intersection point on the ordinate statistically indistinguishable from zero, and the independence of v_z upon [I] clearly point to

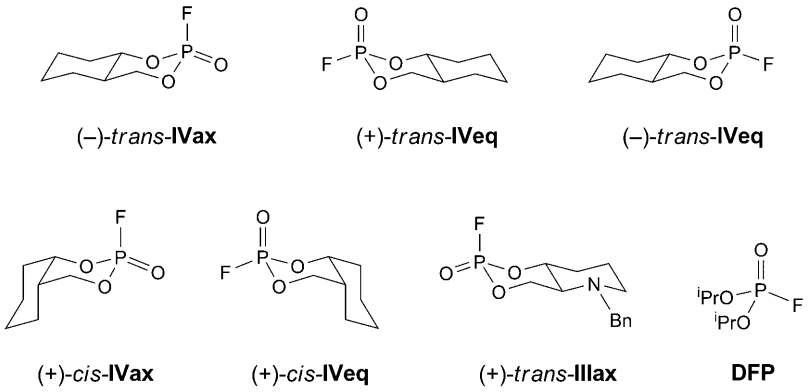

Fig. 6. *The representative 2,4-dioxa-3-fluoro-3-phosphadecalins* (DFP as reference)

Table 4. *Kinetic Data of the Inhibition of AChE with Selected 3-Fluoro-2,4-dioxa-3-phosphadecalins and Assigned Mechanisms,* **DFP** ((i-PrO)$_2$POF) *as Reference.* Numbers indicate best-fit parameters ± standard errors from nonlinear regression, with the exception of (+)-*cis*-**IVeq**, for which the parameters represent values optimized by numerical integration of a set of differential equations corresponding to mechanism **1D** obtained with *Matlab–Simulink* software (www.mathworks.com).

Compound	Kinetic Parameters	Mechanism
(−)-*trans*-**IVax**	$k_3 = 968 \pm 43$ м$^{-1}$ s^{-1}	**1A**
(+)-*trans*-**IVeq**	$K_i = 20.8 \pm 1.3$ μм	**2C**
	$k_4 = 0.037 \pm 0.004$ s^{-1}	
	$k_i = 1280 \pm 150$ м$^{-1}$ s^{-1}	
	$k_6 = 0.014 \pm 0.002$ s^{-1}	
(−)-*trans*-**IVeq**	$K_i = 463 \pm 47$ μм	**2C**
	$k_4 = 0.017 \pm 0.004$ s^{-1}	
	$k_i = 37 \pm 9$ м$^{-1}$ s^{-1}	
	$k_6 = 0.0013 \pm 0.0007$ s^{-1}	
(+)-*cis*-**IVax**	$K_i = 85 \pm 3$ μм	**2A**
	$k_4 = 0.026 \pm 0.001$ s^{-1}	
	$k_i = 306 \pm 16$ м$^{-1}$ s^{-1}	
(+)-*cis*-**IVeq**	$k_3 = 2260$ м$^{-1}$ s^{-1}	**1D**
	$k_5 = 0.026$ s^{-1}	
	$k_6 = 0.00004$ s^{-1}	
(+)-*trans*-**IIIax**	$k_3 = 39 \pm 3$ м$^{-1}$ s^{-1}	**1C**
	$k_6 = 0.00084 \pm 0.00024$ s^{-1}	
DFP	$k_3 = 181 \pm 28$ м$^{-1}$ s^{-1}	**1A**

mechanism **1A** for both of them. With a 5.3 times larger second-order inhibition constant k_3, (−)-*trans*-**IVax** is a significantly better inhibitor than **DFP**.

In *Fig. 8*, two examples of irreversible inhibition occurring in two steps are shown. The progress curves with asymptotes running parallel to the time axis, and the hyperbolic dependence of v_z and λ upon [I], with the trace of λ passing through the origin of the axes, leave no doubts about mechanism **2A** for (+)-*cis*-**IVax**. Instead, (+)-

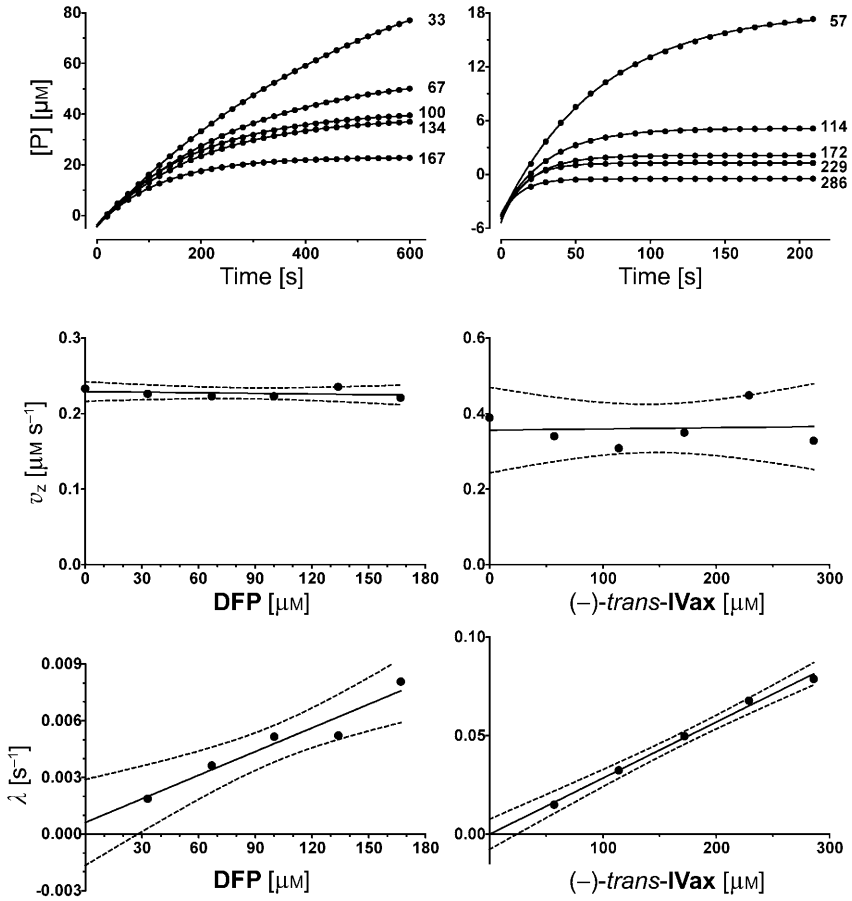

Fig. 7. *Inhibition of AChE by* **DFP** (*left panels*) *and (–)*-trans-**IVax** (*right panels*). In the two *top panels*, only every 20th experimental point is shown for clarity, and solid lines are best-fits according to *Eqn. 8*. Dashed lines around experimental points in the central and bottom panels indicate 95% confidence intervals. Both inhibitors are described by mechanism **1A** with equations shown in *Table 3*, reactions paths in *Scheme 5*, and theoretical curves in *Fig. 4*.

trans-**IVeq** is characterized by progress curves that would suggest a reversible, slow-binding mechanism. However, the chemical nature of the inhibitor and independent evidence from ^{31}P-NMR measurements indicate temporary irreversible inhibition following formation of E–I in a two-step process. E–I is degraded to free enzyme and an inert inhibitor derivative with rate constant $k_6 = 0.014$ s^{-1}, which corresponds to a half-life of 49.5 s, *i.e.*, the covalent E–I compound is almost completely degraded in *ca.* 6 min (7 times the half-life).

The examples in *Fig. 9* illustrate two critical cases that occur when an irreversible inhibitor binds slowly to the enzyme (second-order inhibition constants around 40 M^{-1} s^{-1} in these two examples) and is temporary as well. Since E–I formation is quite a slow process, progress curves can only be measured for a limited time, *i.e.*, until no more

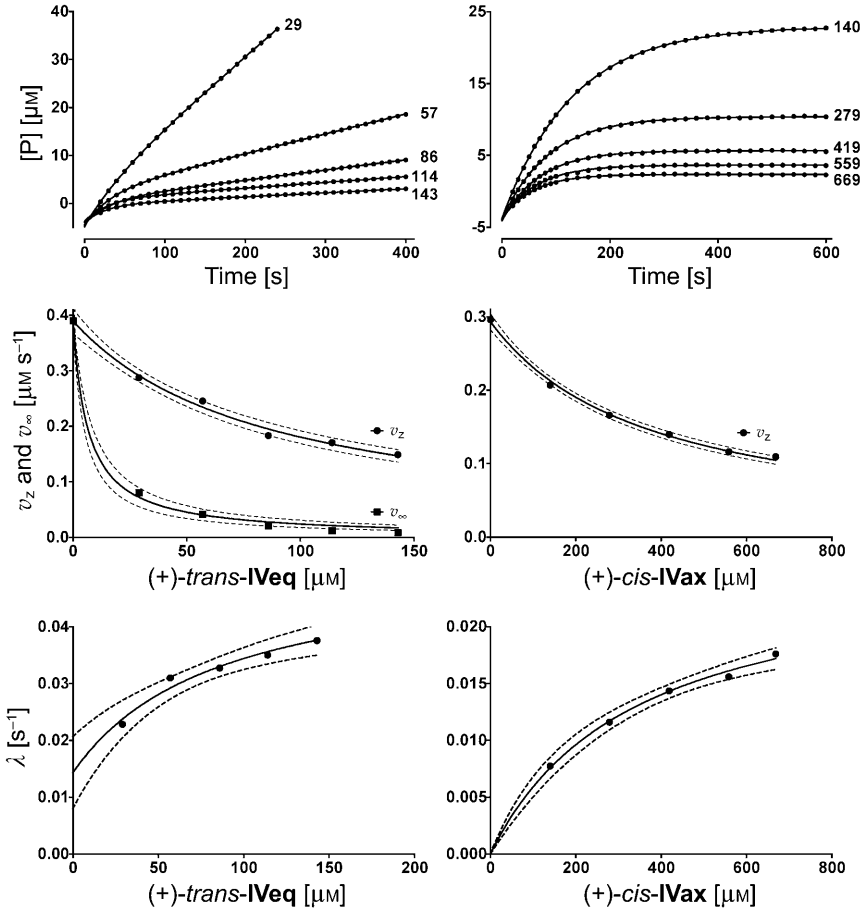

Fig. 8. *Inhibition of AChE by (+)*-trans-**IVeq** (*left panels*) *and (+)*-cis-**IVax** (*right panels*). In the two *top panels*, only every 20th experimental point is shown for clarity, and solid lines are best-fits according to *Eqn. 9* (*left*) or *Eqn. 8* (*right*). Dashed lines around experimental points in the central and bottom panels indicate 95% confidence intervals. (+)-*trans*-**IVeq** is described by mechanism **2C** and (+)-*cis*-**IVax** by mechanism **2A** (*Eqns.* in *Table 2*, reaction paths in *Scheme 4*, and theoretical curves in *Fig. 3*).

than 10–15% of the substrate employed in the assay is used up. As shown, the curves obtained are not very useful because they are incomplete. Of course, reactions can be monitored for longer times, but, in this case, we are faced with two problems. First, excessive substrate consumption violates the necessary condition that the substrate concentration does not appreciably change during the measuring time: the resulting curvature of the progress curves is added to that of irreversible, temporary inhibition. Second, absorbance readings increase excessively causing deviations from the *Lambert–Beer* law. Therefore, a reliable interpretation would be difficult or impossible. Such inhibitors have, of course, little practical interests, but, nevertheless, their kinetics can be interpreted at least qualitatively. Thus, the diagnostic plots for (+)-

trans-**IIIax** (*right panels* in *Fig. 9*) suggest **1C** as the most probable mechanism, although v_z is not perfectly independent of [I]. For (−)-*trans*-**IVeq**, the *left panels* in *Fig. 9* show fits with mechanism **2C** simply because statistical criteria from nonlinear regression of the progress curves suggest a better fit with mechanism **2C** rather than **1C**. With a little portion of common sense, one must, however, admit that there is not much difference between the left and right panels in *Fig. 9*, and that (−)-*trans*-**IVeq** can also be described by mechanism **1C**. Considering mechanism **1C**, the calculated second-order inhibition constant is $k_3 = 30\ \text{M}^{-1}\ \text{s}^{-1}$, and with mechanism **2C**, this is $k_i = 37\ \text{M}^{-1}\ \text{s}^{-1}$, thus a minimal discrepancy considering the technical complexity. This last example shows the limits of the present analysis in decision making, but, fortunately, this is a feature confined to molecules of scarce practical interest.

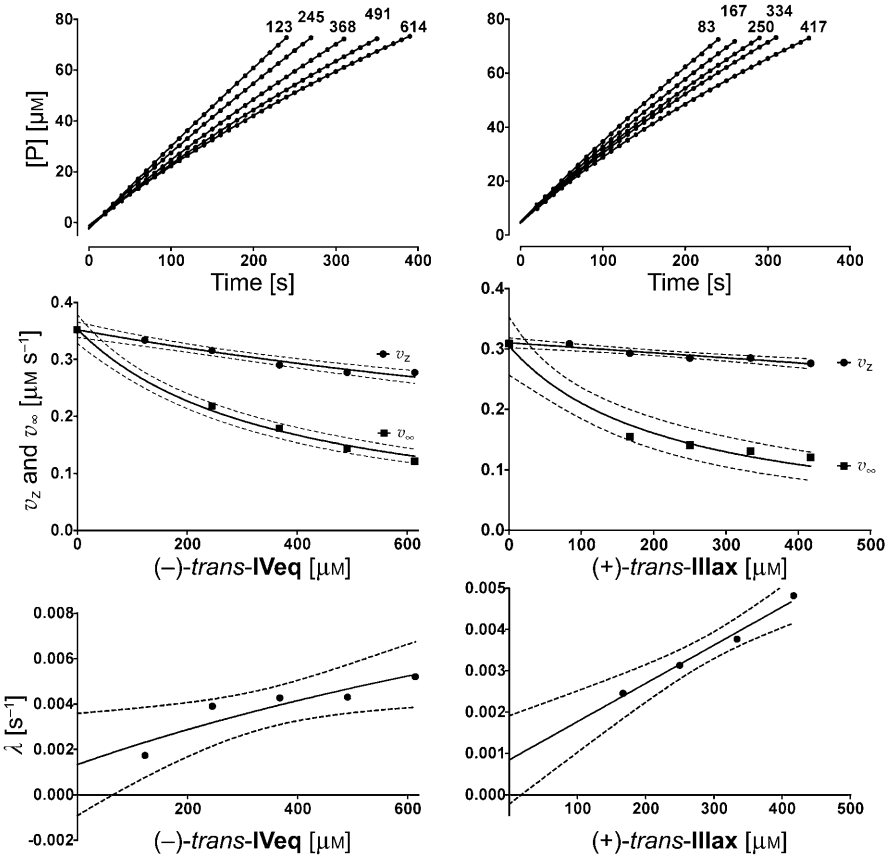

Fig. 9. *Inhibition of AChE by (−)*-trans-**IVeq** (*left panels*) *and (+)*-trans-**IIIax** (*right panels*). In the two *top panels*, only every 20th experimental point is shown for clarity, and solid lines are best-fits according to *Eqn. 9*. Dashed lines around experimental points in the central and bottom panels indicate 95% confidence intervals. (−)-*trans*-**IVeq** is described by mechanism **2C** (*Eqns.* in *Table 2*, reaction paths in *Scheme 4*, and theoretical curves in *Fig. 3*) and (+)-*trans*-**IIIax** by mechanism **1C** (*Eqns.* in *Table 3*, reaction paths in *Scheme 5*, and theoretical curves in *Fig. 4*).

Finally, in *Fig. 10*, a puzzling case is analyzed for compound (+)-*cis*-**IVeq**. Progress curves (*top left panel*) may suggest complete irreversible inhibition according to mechanism **1A**. However, analysis of residuals reveals slight but significantly positive slopes following the exponential phase, which point to either a reversible (**1A-R**) or an irreversible temporary mechanism (**1C**). Another feature is the inconsistent dependency of λ upon inhibitor concentration after primary analysis with *Eqns. 1*, *8*, or *9*. This is now the point where even the best enzyme-kinetic expertise needs help from chemistry. The *right panels* in *Fig. 10* show the instability of (+)-*cis*-**IVeq** as analyzed by ^{31}P-NMR spectroscopy. The signal corresponding to the original molecule ($\delta = -13.34$ ppm) progressively disappears (*lower right panel*), because the molecule is transformed in parallel to the *P(3)*-epimer ((−)-*cis*-**IVax**, $\delta = -12.95$ ppm) and to a hydrolysis product ($\delta = -1.98$ ppm)[5]. Thus, this is an example of unstable inhibitor, and the best-fit curves to experimental data in the *top left panel* of *Fig. 10* were obtained by fitting *Eqn. 16* using a *Maclaurin* expansion to the 10th term under the provisional assumption of mechanism **1B**. However, this equation is valid when the unstable inhibitor is transformed into inert molecules only, whereas the *P(3)*-epimer of (+)-*cis*-**IVeq** also acts as an inhibitor albeit at a much lower rate [14]. Furthermore, we have

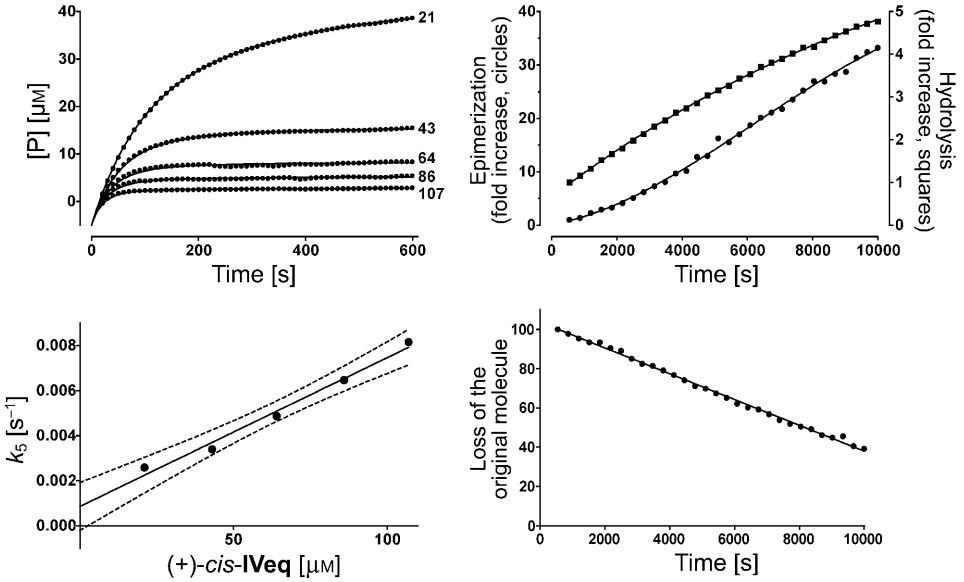

Fig. 10. *Inhibition of AChE by (+)*-cis-**IVeq**. In the top left panel, only every 20th experimental point is shown for clarity, and solid lines are best-fits according to *Eqn. 16*. The decay constant k_5 is not actually constant, but depends on inhibitor concentration (see text for interpretation). The *lower right panel* shows the instability of the molecule as measured by the disappearance with time of its ^{31}P-NMR signal (δ −13.34 ppm), and the *top right panel* the appearance of the epimer (δ −12.95 ppm), as well as of a hydrolysis product, also monitored as ^{31}P-NMR signal (δ −1.98 ppm). The mechanism for this inhibitor is **1D** (*Scheme 5*).

[5]) For further details, see *Exper. Part* and [14].

evidence that E–I also slowly decays, liberating free enzyme and generating another degradation product of the inhibitor. These factors explain why the instability constant k_5 obtained by nonlinear regression is not really constant, but varies with total inhibitor concentration (*Fig. 10*, *lower left panel*) if analysis is performed with *Eqn. 16*, which holds for mechanism **1B**, while the true mechanism is **1D**. Since the contribution of the epimer to total inhibition during the measuring time was found to be minimal, a satisfactory solution of this puzzle comes finally from a combination of nonlinear regression and numerical integration analysis giving the kinetic constants shown in *Table 4*.

4. Conclusions. – The compounds are remarkable irreversible inhibitors (inactivators[4])) of AChE, and several of them are significantly stronger than diisopropyl fluorophosphate (**DFP**) that is generally used as a very potent standard reference (*Table 4*). Moreover, the stereoselectivity of the inhibition reaction is demonstrated for the enantiomers (+)- and (−)-*trans*-**IVeq**. However, since this report places main emphasis on the methodological aspects, we confine ourselves to just presenting distinct examples that demonstrate the easy applicability of our approach. Meanwhile, we have prepared the complete set of the optically active (ee > 99%) 2,4-dioxa-3-fluoro-3-phosphadecalins (type **IV**) [14], and the N-heterocyclic 9-aza- (type **I**) [28], 8-aza- (type **II**) [29], and 7-aza-congeners (type **III**) [30]. Full kinetic data with detailed analyses and interpretations of the inhibition behavior will be presented in following reports [14][28–30].

The authors are indebted to the *Swiss National Science Foundation* and the *Albert-Böni Foundation* (*A. B.*) for their generous financial support.

Experimental Part

1. *General.* The preparation and the full characterization of the 3-substituted 3-phosphadecalins of the types **I**–**IV** are described in [1][14][28–30]. Acetylcholinesterase (AChE) from *Electrophorus electricus* (electric eel), *Sigma C-2888*, type *V-S*, lyophilized powder ≥ 1000 units/mg protein (lots 39 H7402, 103K7651, 129F8080, 228F8040); acetylthiocholine (ATC), *Fluka 01480 BioChemika*; 5,5′-dithiobis(2-nitrobenzoic acid-3,3′-6) (DTNB; *Ellman*'s reagent [27]), *Fluka 43760 BioChemika*; diisopropyl fluorophosphate (DFP), *Fluka 38399*, *pract.*; H_2O, *Fluka 95304* (HPLC quality); MeCN, *Fluka 00695 puriss.* abs. (over molecular sieves); NaCl, *Fluka 71378 BioChemika MicroSelect*; $NaH_2PO_4 \cdot H_2O$, *Merck 6346 p.a.*; $Na_2HPO_4 \cdot 2\ H_2O$, *Merck 6580 p.a.*; *Pluronic F-68*, *Sigma P-1300* (lot 88 H1000); *Tris* buffer, *Fluka 93349 BioChemika MicroSelect*. Volumes ≤ 1 ml were measured accurately with microliter pipettes *Socorex S+* (100–1000 µl) and *Socorex Autoclavable Calibra 822* (10–100 µl, 1–10 µl), and volumes < 1 ml by diluting in volumetric flasks. pH Determinations: *Knick Portamess 762 Calimatic*, electrode: *Mettler InLab 423 S7*; calibration: *Mettler* standard buffers pH 4.01 and pH 7.00; electrolyte: *Mettler* standard, 3M KCl sat. with AgCl; measurements at 22°, accuracy ± 0.02 pH units. Enzyme kinetic progress curves and photometric titration of the active sites of AChE: *Hewlett-Packard 8452A* diode array spectrophotometer with *HP 89532A* UV/VIS Software (Rev. A.00.00). Curve-fitting and data analyses were performed with OriginPro 7.5G SR3 v.7.5853 (www.originlab.com) and *GraphPad Prism* version 5.00 for Windows, *GraphPad* Software, San Diego California USA (www.graphpad.com).

2. *Enzyme Kinetics.* 2.1. *Phosphate Buffer pH 7.00.* Soln. *A:* $Na_2HPO_4 \cdot 2\ H_2O$ (4.45 g), NaCl (1.46 g), and *Pluronic F-68* (25 mg) were dissolved in H_2O (250 ml). Soln. *B:* $NaH_2PO_4 \cdot H_2O$ (6.90 g), NaCl (2.92 g), and *Pluronic F-68* (25 mg) were dissolved in H_2O (500 ml). The solns. were adjusted to pH 7.00 ± 0.02 by mixing. Prior to use, the buffer was filtered (*TRP* syringe filter, max. 0.5 MPa, PES membrane 0.22 µ, gamma sterilized, free of pyrogens).

2.2. *AChE Solns.* AChE (1 mg) was dissolved in the phosphate buffer pH 7.00 (1 ml), thoroughly mixed, and stored at 5° (stock soln.). To the phosphate buffer (5 ml), AChE stock soln. (5 µl) was added and thoroughly mixed. The soln. (1 ml) was diluted to 10 ml with phosphate buffer. Such a soln. could be used for the determination of K_m and one assay series.

2.3. *ATC Soln.* ATC (22.6 mg) was dissolved in phosphate buffer (1 ml (→ 78 mM)) and thoroughly mixed. The solns. were freshly prepared prior to use and stored at 0° (ice bath).

2.4. *DTNB Soln.* DTNB (15 mg) was dissolved in phosphate buffer (2 ml (→ 19 mM)) and well mixed prior to use.

2.5. *Inhibitor Soln.* (representative example). The respective 3-substituted 3-phosphadecalin (3.5 mg) was dissolved in abs. MeCN (200 µl). From this stock soln., a dilution series was prepared to yield five different concentrations. The total volume of each assay was 25 µl.

2.6. *Determination of* K_m. Prior to each assay series, the *Michaelis* constant (K_m) was determined under the assay conditions (instead of an inhibitor, MeCN (25 µl) was added). The linear increase of the absorption was monitored at 410–414 nm at five different concentrations of the substrate (ATC; [S] = [ATC] from 100–500 µM). The *Michaelis–Menten* equation was fitted to the steady-state rates to calculate K_m by nonlinear regression, which was always in the range of 160 µM.

2.7. *Assay.* In a polystyrene cell ($d = 10$ cm), phosphate buffer pH 7.00 (2 ml), DTNB soln. (100 µl), and ATC soln. (20 µl) were mixed and thermostatted at 25°. The inhibitor soln. (25 µl, known [I]) was added. At $t = 0$, the AChE soln. (1 ml) was added, and the mixture gently mixed for 20 s. After 20 s, the monitoring of the absorption automatically started, and 600 data points were collected for 10 min at various concentrations of the inhibitors. As in the K_m determinations, the total volume was 3.15 µl, the concentration of the substrate [S] = 502 µM. Per inhibitor, at least five measurements with different inhibitor concentrations were performed, the smallest one being *ca.* 1/5–1/10 of the largest one.

2.8. *Titration of the Active Sites of AChE.* The concentrations of the active sites in the AChE samples were determined photometrically by titration with *N,N*-dimethyl-*O*-(2-nitrophenyl)carbamate according to [31] at 25°. In this reaction, the enzyme hydrolyzes an equimolar amount of 2-nitrophenolate that is monitored at 415 nm. The concentration is determined by means of a calibration line that was established with 2-nitrophenolate under identical reaction conditions. *Phosphate Buffer pH 7.70.* Soln. *A:* $NaH_2PO_4 \cdot H_2O$ (39.3 mg), NaCl (58.4 mg), and *Pluronic F-68* (1 mg) were dissolved in H_2O (10 ml). Soln. *B:* $Na_2HPO_4 \cdot 2\,H_2O$ (1.25 g), NaCl (584 mg), and *Pluronic F-68* (10 mg) were dissolved in H_2O (100 ml). The solns. were adjusted to pH 7.70 ± 0.02 by mixing. *AChE Solutions.* AChE (1 mg) was dissolved in the phosphate buffer pH 7.70 (250 µl). *Titration* (representative example for AChE lot 129F8080). To phosphate buffer pH 7.70 (2 ml) in a polystyrene cell ($d = 10$ cm), a soln. (50 µl) of *N,N*-dimethyl-*O*-(2-nitrophenyl)carbamate (7.57 mg/ml in abs. MeCN) was added, and the absorption was measured at 415 nm for 5 min. Then, the soln. (50 µl) of AChE was added, and the progress curve was monitored for 15 min. The procedure was repeated twice to confirm its reproducibility. Data analysis showed the concentration of active sites to be $1.75 \cdot 10^{-8}$ mol/mg.

2.9. *Data Analysis and Assignment of the Inhibition Mechanisms. Eqns. 8* or *9* were fitted to progress curves by nonlinear regression using *GraphPad Prism* version 5.00 for Windows, *GraphPad* Software, San Diego, California USA (www.graphpad.com). The runs test and analysis of residuals were performed to monitor significant deviations from the model. λ, v_z, and v_∞ (where appropriate) obtained as the parameters of this primary analysis were plotted *vs.* the inhibitor concentration. The dependence of λ on [I] was analyzed with models **2A**, **2C**, **1A**, and **1C** (*Eqns.* in *Tables 2* and *3*), and model discrimination was performed by analysis of variance of the difference between the sum of squares (extra sum-of-squares test), and calculation of *F* ratios and *p* values. The dependence of v_z and v_∞ on [I] was analyzed using the appropriate *Eqns.* in *Tables 2* and *3*. When primary fittings to progress curves using *Eqns. 8* and *9* were inconsistent, and there was no clear dependency of λ upon [I], mechanism **1B** was considered and *Eqn. 16* was fitted to data. ^{31}P-NMR Analyses confirmed in these cases instability of the inhibitors under the assay conditions resulting in hydrolysis and/or epimerization of the molecule. Data shown in *Table 4* report the mechanism and the best-fit inhibition constants with associated standard error from regression analysis.

3. *^{31}P-NMR Experiments. Stability of (+)*-cis-**IVeq**. 3.1. *General.* The ^{31}P{^{1}H}-NMR spectra were recorded at 161.98 MHz on a *Bruker AV2-400* spectrometer at 300 K (δ in ppm, *J* in Hz).

3.2. *Solvents.* Soln. *A:* $Na_2HPO_4 \cdot 2\,H_2O$ (445 mg), NaCl (146 mg), and *Pluronic F-68* (2.5 mg) were dissolved in D_2O (25 ml). Soln. *B:* $NaH_2PO_4 \cdot H_2O$ (690 mg), NaCl (292 mg), and *Pluronic F-68* (2.5 mg) were dissolved in D_2O (50 ml). The solns. were adjusted to pH*[6]) 7.00 ± 0.02 by mixing.

3.3. *Data.* (+)-*cis*-**IVeq**: δ −13.34 (*d*, ^1J(P,F) = 986); (−)-*cis*-**IVax**: δ −12.95 (*d*, ^1J(P,F) = 1003). The hydrolysis product (2,4-dioxa-3-hydroxy-3-phosphabicyclo[4.4.0]decane 3-oxide) appeared at δ −1.98 ppm (*s*), and inorg. phosphate was detected at δ 2.11 (*s*)[5]).

Appendix. – *Symbols and Nomenclature Conventions Used in This Article: d* = Displacement of a progress curve from the zero value; E = free enzyme; EI = adsorptive enzyme–inhibitor or enzyme–inactivator[4]) complex; E·I = reversible enzyme–inhibitor complex (competitive with substrate); E–I = irreversibly, covalently modified enzyme (competitive with substrate); ES = enzyme–substrate complex; I = inhibitor (reversible inhibitor or irreversible modifier (inactivator[4]))); I′ = chemically transformed I (*e.g.*, by hydrolysis), which does no longer bind to the enzyme; I* = enzymatically transformed I, which does no longer bind to the enzyme; k_1, k_3 = second-order rate constants; k_{-1}, k_2, k_{-3}, k_4, k_5, k_6, k_7, k_{-7} = first-order rate constants; $K_i = k_{-3}/k_3$ = dissociation constant; $k_i = k_4/K_i$ = second-order inhibition constant; P = product(s); S = substrate; v_s = reaction rate at steady-state; v_z = reaction rate at time zero (t = 0); v_0 = reaction rate in the absence of modifiers; λ = first-order rate constant of the exponential phase for the formation of E–I or EI; [X] = concentration of the free species X in mol dm^{-3}; $[X]_t$ = total concentrations of species X; $[X]_z$ = concentrations of species X at t = 0.

REFERENCES

[1] S. Furegati, W. Ganci, F. Gorla, U. Ringeisen, P. Rüedi, *Helv. Chim. Acta* **2004**, *87*, 2629.
[2] W. Ganci, E. J. M. Meier, F. Merckling, G. Przibille, U. Ringeisen, P. Rüedi, *Helv. Chim. Acta* **1997**, *80*, 421; S. Furegati, W. Ganci, G. Przibille, P. Rüedi, *Helv. Chim. Acta* **1998**, *81*, 1127.
[3] M. J. Stöckli, P. Rüedi, *Helv. Chim. Acta* **2001**, *84*, 106; M. J. Stöckli, P. Rüedi, *Helv. Chim. Acta* **2007**, *90*, 2058.
[4] W. N. Aldridge, *Biochem. J.* **1950**, *46*, 451.
[5] A. R. Main, W. C. Dauterman, *Nature* **1963**, *4880*, 551; A. R. Main, *Science* **1964**, *114*, 992.
[6] G. Hart, R. D. O'Brien, *Biochemistry* **1973**, *12*, 2940.
[7] H. A. Berman, K. Leonard, *J. Biol. Chem.* **1989**, *264*, 3942; H. A. Berman, M. M. Decker, *J. Biol. Chem.* **1989**, *264*, 3951; H. A. Berman, K. Leonard, *J. Biochem.* **1990**, *29*, 10640, and refs. cit. therein.
[8] F. A. Merckling, '^{31}P-NMR-spektroskopische Untersuchungen der Inhibierung von Acetylcholinesterase mit Organophosphaten', Ph.D. Thesis, University of Zurich, 1993.
[9] U. Ringeisen, 'Synthese und Charakterisierung von N-heterocyclischen Organophosphaten als Inhibitoren der Acetylcholinesterase', Ph.D. Thesis, University of Zurich, 1996.
[10] W. M. Ganci, 'Untersuchung der Wechselwirkungen von Serinhydrolasen mit Organophosphaten: Synthese kationischer N-Heterocyclen als Acetylcholin-Mimetika und ^{31}P-NMR-Spektroskopie von Enzym-Inhibitoraddukten', Ph.D. Thesis, University of Zurich, 1998.
[11] S. Furegati, 'Synthese von konformativ definierten Organophosphat-Acetylcholinmimetika zur Untersuchung der Inhibition von Acetylcholinesterase', Ph.D. Thesis, University of Zurich, 2002.
[12] F. Gorla, 'Internal Progress Report', University of Zurich, 1998.
[13] S. Furegati, F. Gorla, A. Linden, P. Rüedi, *Chem.-Biol. Interact.* **2005**, *157–158*, 415.
[14] M. Wächter, 'Herstellung optisch aktiver Organophosphate mit *cis*- und *trans*-Decalingerüst zur Untersuchung der Inhibition von Acetylcholinesterase', M.Sc. Thesis, University of Zurich, 2005; M. Wächter, P. Rüedi, *Chem. Biodiversity* **2009**, *6*, 283.
[15] S. E. Szedlacsek, R. G. Duggleby, *Methods Enzymol.* **1995**, *249*, 144.
[16] A. Baici, *Biol. Chem.* **1998**, *379*, 1007.
[17] L. H. Easson, E. Stedman, *Proc. R. Soc. London, Ser. B* **1936**, *121*, 142.

---

[6]) pH* is the nominal pH value of a soln. in D_2O read on a pH-meter calibrated with standard buffers in H_2O; pD ≈ pH + 0.4 [32].

[18] W. W. Ackerman, V. R. Potter, *Proc. Soc. Exp. Biol. Med.* **1949**, *72*, 1.
[19] R. Kitz, I. B. Wilson, *J. Biol. Chem.* **1962**, *237*, 3245.
[20] W. X. Tian, C. L. Tsou, *Biochemistry* **1982**, *21*, 1028; C. L. Tsou, *Adv. Enzymol. Relat. Areas Mol. Biol.* **1988**, *61*, 381.
[21] P. J. Gray, R. G. Duggleby, *Biochem. J.* **1989**, *257*, 419.
[22] K. F. Tipton, in 'Enzyme Inhibitors as Drugs', Ed. M. Sandler, McMillan, London, 1980, p. 1.
[23] C. M. Topham, *J. Theor. Biol.* **1990**, *145*, 547.
[24] C. Frieden, *J. Biol. Chem.* **1970**, *245*, 5788.
[25] S. Cha, *Biochem. Pharmacol.* **1975**, *24*, 2177.
[26] J. F. Morrison, *Trends Biochem. Sci.* **1982**, *7*, 102; J. F. Morrison, S. R. Stone, *Comments Mol. Cell. Biophys.* **1985**, *2*, 347.
[27] G. L. Ellman, K. D. Courtney, V. Andres Jr., R. M. Featherstone, *Biochem. Pharmacol.* **1961**, *7*, 88.
[28] P. G. Lorenzetto, A. Strehler, P. Rüedi, *Helv. Chim. Acta* **2006**, *89*, 3023; P. G. Lorenzetto, 'Synthese und Charakterisierung der enantiomerenreinen 9-Aza-3-phosphadecaline als Acetylcholin-Mimetika', Ph.D. Thesis, University of Zurich, 2009; P. G. Lorenzetto, A. Linden, M. Wächter, P. Rüedi, *Helv. Chim. Acta*, in preparation.
[29] C. Clerc, 'Synthese und Charakterisierung von enantiomerenreinen N-heterocyclischen Phosphadecalinen als Inhibitoren von Acetylcholinesterase', Ph.D. Thesis, University of Zurich, 2008; C. Clerc, P. Rüedi, *Helv. Chim. Acta*, in preparation.
[30] M. Wächter, 'Herstellung von optisch aktiven Organophosphaten mit *cis*- und *trans*-Decalingerüst zur Untersuchung der Inhibition von Acetylcholinesterase mittels Enzymkinetik und ^{31}P-NMR-Spektroskopie', Ph.D. Thesis, University of Zurich, submitted; M. Wächter, P. Rüedi, *Helv. Chim. Acta*, in preparation.
[31] M. L. Bender, M. L. Begué Cantón, R. L. Blakeley, L. J. Brubacher, J. Feder, C. R. Gunter, F. J. Kézdy, J. V. Killheffer Jr., T. H. Marshall, C. G. Miller, R. W. Roeske, J. K. Stoops, *J. Am. Chem. Soc.* **1966**, *88*, 5890.
[32] A. Krezel, W. Bal, *J. Inorg. Biochem.* **2003**, *98*, 161.

Received October 10, 2008